

---

This is an electronic reprint of the original article.  
This reprint may differ from the original in pagination and typographic detail.

Ila, M.; Louhi-Kultanen, M.

## Purification of monoethylene glycol by melt crystallization

*Published in:*  
Chemical Engineering Science

*DOI:*  
[10.1016/j.ces.2023.118601](https://doi.org/10.1016/j.ces.2023.118601)

Published: 15/05/2023

*Document Version*  
Publisher's PDF, also known as Version of record

*Published under the following license:*  
CC BY

*Please cite the original version:*  
Ila, M., & Louhi-Kultanen, M. (2023). Purification of monoethylene glycol by melt crystallization. *Chemical Engineering Science*, 272, Article 118601. <https://doi.org/10.1016/j.ces.2023.118601>

---

This material is protected by copyright and other intellectual property rights, and duplication or sale of all or part of any of the repository collections is not permitted, except that material may be duplicated by you for your research use or educational purposes in electronic or print form. You must obtain permission for any other use. Electronic or print copies may not be offered, whether for sale or otherwise to anyone who is not an authorised user.



# Purification of monoethylene glycol by melt crystallization

M. Ila, M. Louhi-Kultanen \*

Department of Chemical and Metallurgical Engineering, School of Chemical Engineering, Aalto University, P.O. Box 16100, FI-00076 Aalto, Finland



## HIGHLIGHTS

- Layer melt crystallization of monoethylene glycol was investigated.
- Impurity under study was 1,2-pentanediol and solvent additive acetone.
- Thermodynamic driving forces with and without solvent additive were determined.
- Crystallization kinetics affects purity of final product.

## ARTICLE INFO

### Article history:

Received 16 December 2022  
 Received in revised form 17 February 2023  
 Accepted 28 February 2023  
 Available online 3 March 2023

### Keywords:

Purification  
 Melt crystallization  
 Assisting solvent  
 Thermodynamics

## ABSTRACT

Separation of glycols with close boiling points and relatively high viscosity at their melting point is a challenge in the production of high purity products downstream of biorefinery processes. In this work, the efficiency of the layer melt crystallization process with acetone as the assisting solvent was evaluated for a mixture of monoethylene glycol and 1,2-pentanediol. Solid-liquid equilibrium was measured and modelled with the NRTL and modified UNIFAC group-contribution models to evaluate the thermodynamic driving force of crystallization. Layer melt crystallization was conducted to determine the effect of solvent composition on purity, distribution coefficient of impurity, crystal growth rate, and yield at different operating conditions. Addition of the solvent altered the thermodynamics and kinetics of crystallization, thereby altering the purity level of the final product. An effective distribution coefficient of impurity between 0.1 and 0.6 in one-step crystallization was obtained, depending on the solvent composition and the applied operating conditions.

© 2023 The Author(s). Published by Elsevier Ltd. This is an open access article under the CC BY license (<http://creativecommons.org/licenses/by/4.0/>).

## 1. Introduction

Purification in downstream of biorefineries is an important stage in the production of value-added products. Monoethylene glycol (MEG) is an important raw material with high demand in many industrial sectors, such as the production of polyester fibers and resins, and hydrogen fuel and the production of chemicals from its oxidation (Yue et al., 2012). Distillation has been widely used as a separation and purification technique. Nevertheless, many recent studies on mixtures of glycols show that separation via traditional distillation is difficult due to their close boiling points, or azeotrope formation (Li et al., 2018; Yu et al., 2016; Zhang et al., 2013).

In this work, 1,2-pentanediol (PD) as the impurity was investigated in the production of pure MEG. To the best of our knowledge, experimental vapor-liquid equilibrium (VLE) data for this binary

mixture have not been reported in the literature. In the present work, the VLE data were estimated at atmospheric pressure by using the modified UNIFAC Dortmund model via the Aspen Plus V11.0 simulation program, which indicates the formation of a minimum azeotrope. Therefore, the production of high purity MEG from this system through the traditional distillation process cannot be obtained. Melt crystallization is an alternative technique for the production of high purity compounds from organic systems. This method is a suitable alternative for separation of systems with close boiling compounds (Cong et al., 2015; Feng et al., 2023; Micovic et al., 2013). Wang et al. (2020) studied the separation potential of layer crystallization for the purification of ethylene glycol from short-chain glycol impurities, 1,2-butanediol and 1,2-propanediol, which are the major impurities coproduced during the production of ethylene glycol from coal-based syngas. It was shown that, depending on the impurity content of the feed, multi-stage crystallization and a post-treatment process are required to achieve the desired purity of the final product, which may lead to low yield due to the loss of ethylene glycol through these batch processes.

\* Corresponding author.

E-mail address: [marjatta.louhi-kultanen@aalto.fi](mailto:marjatta.louhi-kultanen@aalto.fi) (M. Louhi-Kultanen).

## Nomenclature

$G$	crystal growth rate (m/s)	$\gamma^*$	liquid activity coefficient, saturated (–)
$G_{ij}$	coefficient as defined in Equation (3)	$\rho$	density (kg/m <sup>3</sup> )
$\Delta H_m$	enthalpy of fusion (J/mol)	$\tau_{ij}$	coefficient as defined in Equation (4)
$k_{eff}$	effective distribution coefficient (–)	$\Delta\mu$	chemical potential driving force (J/mol)
$m_{cry}$	mass of crystal (kg)		
$m$	total mass of melt (kg)	<i>Sub- and superscripts</i>	
$m'$	mass of melt on solvent-free basis (kg)	$c$	coolant
$x$	liquid-phase mol fraction (–)	$f$	feed
$y$	vapor-phase mol fraction (–)	$i$	component i
$x'$	mol fraction on solvent-free basis (–)	$m$	melt
$r$	radius (m)	$s$	solvent
$R$	ideal gas constant (J/mol.K)		
$T$	temperature (K)	<i>Abbreviations</i>	
$T_m$	melting point (K)	GC	gas chromatography
$w$	mass fraction (–)	MEG	monoethylene glycol
$w'$	mass fraction on solvent-free basis (–)	PD	1,2-pentanediol
		SLE	solid-liquid equilibrium
		VLE	vapor-liquid equilibrium
<i>Greek symbols</i>			
$\alpha_{ij}$	nonrandomness constant for binary ij interactions		
$\gamma$	liquid activity coefficient (–)		

On the other hand, solvent-aided melt crystallization has attracted interest in the case of relatively viscous mixtures. Eisenbart & Ulrich (2015) used an assisting solvent to enhance the crystal growth kinetics by reducing the viscosity of the glycerol-water system. It was shown that adding the appropriate type and amount of solvent reduced the distribution coefficients of impurities at reasonable growth rates compared to the binary mixture.

Nonetheless, separation efficiency of solvent-aided crystallization is dependent on the choice and amount of the solvent. In this work the separation efficiency of layer melt crystallization in the purification of MEG from the binary glycol mixture as well as in the presence of an assisting solvent was evaluated. Acetone, a representative of a polar aprotic solvent with relatively low viscosity and high vapor pressure is suggested as an assisting agent for crystallization. The higher vapor pressure of the solvent can reduce the operating costs associated with solvent recycling. Layer melt crystallization was conducted to investigate the effect of solvent composition on the thermodynamics and kinetics viewpoint of crystallization as well as the purity and process yield under different operating conditions.

## 2. Theoretical section

### 2.1. Thermodynamic driving force of crystallization

The fundamental driving force for crystallization is defined as the difference between the chemical potential of the solute in the liquid and solid phase. The dimensionless driving force of crystallization can be expressed as:

$$\frac{\Delta\mu_i}{RT} = \ln \left( \frac{x_i \gamma_i}{x_i^* \gamma_i^*} \right) \quad (1)$$

The chemical activity-based supersaturation expression is superior to the common concentration-based supersaturation, particularly in a non-ideal system where the activity coefficient ratio ( $\gamma_i/\gamma_i^*$ ) greatly deviates from unity (Mullin, 2001). The activity coefficient of the liquid phase at equilibrium ( $\gamma_i^*$ ) can be estimated by

group contribution models or determined by correlation of semi-empirical models with solid-liquid equilibrium (SLE) data. The activity coefficient in the supersaturated liquid phase ( $\gamma_i$ ) can be estimated from equilibrium data, assuming that the activity coefficient of the liquid phase is a weak function of temperature (Valavi et al., 2016).

### 2.2. Calculation of phase diagram and liquid phase activity coefficients

Predictive and semi-empirical activity coefficient models can be used to estimate the SLE and liquid phase activity coefficients. The predictive capabilities of the modified UNIFAC-Dortmund (UNIFAC-DMD) (Gmehling et al., 1993) and NIST-modified UNIFAC group contribution models (Kang et al., 2015, 2017) were evaluated to determine the activity coefficient of the liquid phase in the binary and ternary systems of 1,2-ethanediol/1,2-pentanediol and 1,2-ethanediol/1,2-pentanediol/acetone. In the modified UNIFAC-DMD model, the ethylene glycol consists of one group of DOH (diol); 1,2-pentanediol is defined as one CH<sub>3</sub>, three CH<sub>2</sub>, one CH, one OH (primary), and one OH (secondary) groups; and the acetone is characterized by one CH<sub>3</sub> and CH<sub>3</sub>CO groups.

The NIST-modified UNIFAC model has been developed to show improved prediction of vapor-liquid equilibrium data for diols. This model provides new subgroups for diols which contribute the effect of steric hindrances due to the presence of multiple hydroxyl groups attached to the adjacent carbon in their molecular structure. In this work, the extrapolation of activity coefficients at crystallization temperatures was evaluated for the NIST-modified UNIFAC model. According to the definition of the new subgroups, the 1,2-pentanediol is comprised of one CH<sub>3</sub>, two CH<sub>2</sub> and one (–CH(OH)–CH<sub>2</sub>(OH)) groups. The details of these models can be found elsewhere (Kang et al., 2015, 2017).

Furthermore, for reliable estimation of the activity coefficient, the NRTL model (Renon & Prausnitz, 1968) can be used for the correlation of SLE measured data. To apply the NRTL model, a regression was performed to optimize the binary interaction parameters. The parameters were obtained by minimizing the sum of the squares of differences between experimental and calculated tem-

peratures. In this model the logarithm of the activity coefficient and binary interaction parameters are expressed by:

$$\ln \gamma_i = \frac{\sum_{j=1}^N \tau_{ji} G_{ji} x_j}{\sum_{k=1}^N G_{ki} x_k} + \sum_{j=1}^N \frac{x_j G_{ij}}{\sum_{k=1}^N G_{kj} x_k} \left[ \tau_{ij} - \frac{\sum_{k=1}^N x_k \tau_{kj} G_{kj}}{\sum_{k=1}^N G_{kj} x_k} \right] \quad (2)$$

$$G_{ij} = \exp(-\alpha_{ij} \tau_{ij}) \quad (3)$$

$$\tau_{ij} = a_{ij} + \frac{b_{ij}}{T} \quad (4)$$

$$\alpha_{ij} = \alpha_{ji} \quad (5)$$

The relation between the activity coefficient of the liquid phase and SLE can be described based on the equal chemical potential of each component for the solid and liquid phases. A simplified relationship between the liquid phase composition, activity coefficient, and equilibrium temperature with the assumption of the formation of pure solid phase can be expressed by (Walas, 1985):

$$x_i^* \gamma_i^* = \exp \left[ \frac{\Delta H_m}{R} \left( \frac{1}{T_m} - \frac{1}{T} \right) \right] \quad (6)$$

### 3. Experimental

#### 3.1. Chemicals

The ethylene glycol and acetone with 99.5% purity were purchased from Thermo Scientific. The 1,2-pentanediol (>98.0%) was purchased from TCI Chemicals. Sodium chloride (>99.0%, Sigma-Aldrich) was used for calibration purposes.

#### 3.2. Seed production

Pure ethylene glycol crystals were formed by scratching the glass in contact with the solution at a temperature of  $-30$  °C. MEG can also undergo spontaneous crystallization after remaining at  $-45$  °C for 15 to 30 min. Wang et al. (2020) generated ethylene glycol seeds from a binary mixture with a controlled cooling strategy.

#### 3.3. Solid-liquid equilibrium measurement

The setup consists of a 250 mL jacketed vessel connected to a Lauda ECO RE 1050 thermostat. The aqueous solution coolant of 60 wt.% ethylene glycol was circulated inside the jacket. An anchor impeller with a rotation speed of 25 rpm was used to provide a uniform temperature inside the mixture. The temperature of the solution was measured with a thermocouple. The precision of the thermocouple was evaluated by measuring the freezing point of two aqueous solutions of 2% NaCl and 2% MEG. The measured data showed less than 0.1 K deviation from the literature data (Haynes et al., 2017). To obtain SLE data for binary and ternary compound systems, the crystallization temperature of various melt compositions was measured according to the following approach: 1) adjusting the coolant temperature to obtain a specific undercooling degree in the melt, and 2) addition of a seed to the mixture to induce crystallization in a controlled manner. The temperature of the melt rises to a constant value due to the released heat of crystallization. The equilibrium temperature was determined as the average temperature within the time with a temperature change of less than  $\pm 0.02$  K. The time during which the temperature remains stable depends on the applied undercooling degree. To ensure the equilibrium state, the experiments were repeated by applying lower undercooling degrees (see Fig. 1).

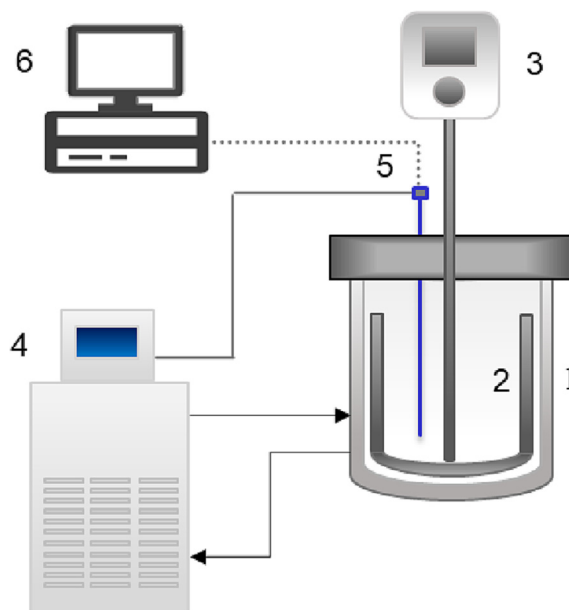


Fig. 1. Schematic overview of suspension crystallization setup for SLE measurement: (1) double jacket, (2) anchor impeller, (3) mixer, (4) thermostat, (5) thermocouple, (6) computer.

#### 3.4. Layer melt crystallization

Layer crystallization was performed on the cold surface of a beaker with an inner diameter of 31 mm, which was immersed inside the cooling bath of the Lauda ECO RE 1050 thermostat (Fig. 2.a). The cold surface temperature was controlled by adjusting the temperature of the cooling medium ( $T_c$ ) containing 60 wt.% aqueous ethylene glycol solution. A thermocouple located at the center and top of the crystal surface was used to monitor the temperature of the melt ( $T_m$ ) at different operating temperatures. The difference between the  $\Delta T_c$  and  $\Delta T_m$  (Fig. 2.b) indicated that the system has not reached equilibrium at the applied cooling rates. This can imply the possibility of kinetic incorporation of impurities into the crystal layer.

The first step in layer crystallization was to produce a thin layer of crystalline MEG at the bottom of the beaker to initiate the crystal growth vertically above the seed layer. Crystallization was started by adding the solution at 0.2 K below its freezing point ( $T_f^*$ ). The temperature of the melt was maintained at this temperature for 10 min. Subsequently, the coolant temperature was reduced to the intended final temperature by applying constant cooling rates. At the end of the experiment, the mother liquor was separated from the crystal layer and the mass of the solid phase was measured. The concentration of the impurity and solvent in the melted crystal layer was determined by gas chromatography.

#### 3.5. Analytics

Gas chromatography (GC-FID, Agilent 6890) equipped with a flame ionization detector (320 °C) and HP1 (60 m  $\times$  0.25 mm  $\times$  1  $\mu$  m) column was used to measure the purity of the final crystalline products. Helium was used as the carrier gas at a constant flow rate of 20 mL/min. The oven temperature was set to 140 °C for 10 min. Subsequently, the temperature was raised to 250 °C with a heating rate of 30 °C/min and kept at the final temperature for 10 min.

The composition of each sample was determined using a calibration line based on the known mass ratio of the solute and impu-

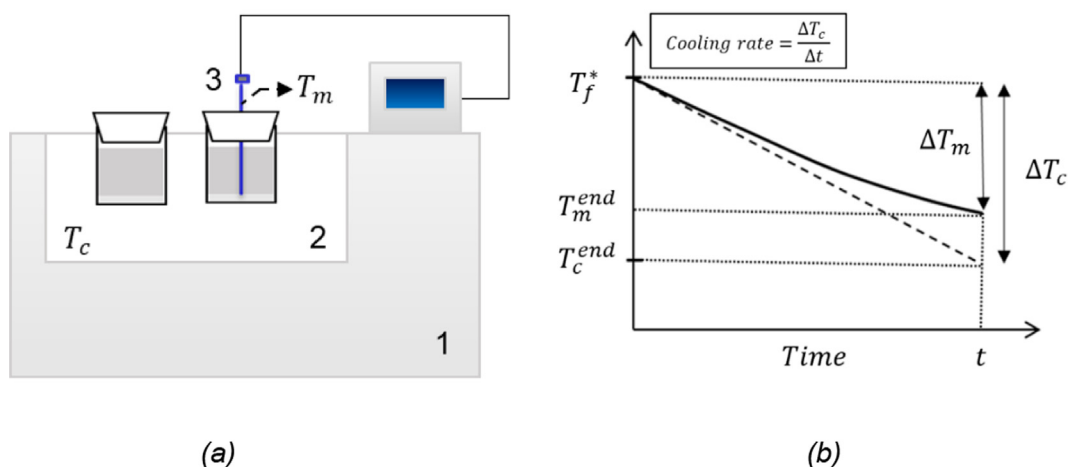


Fig. 2. Schematic overview of layer melt crystallization setup: (a) thermostat (1), coolant (2), thermocouple (3) and (b) sketch of experimental cooling procedure.

rity against the ratio measured by GC. In this work, the purity was reported on a solvent-free basis:

$$w'_{MEG} = \frac{w_{MEG}}{w_{impurity} + w_{MEG}} \quad (7)$$

Viscosities at crystallization temperatures were measured using an Anton Paar Physica MCR 301 rheometer with concentric cylinder geometry and a shear rate of  $100 \text{ s}^{-1}$ .

## 4. Results and discussion

### 4.1. Thermodynamic modeling and prediction of VLE and SLE data

The VLE phase diagram was predicted using Aspen Plus V 11.0 software. The following methods were defined for predicting vapor-liquid equilibrium data for a binary mixture of MEG and 1,2-pentanediol: The UNIFAC-DMD model was used as the property method and for calculating the activity coefficient in the liquid phase. The functional groups for the 1,2-pentanediol molecule were entered manually based on the UNIFAC-DMD functional groups. The Redlich-Kwong-Soave equation of state model with the Boston-Mathias modification (ESRKS) was selected for calculating the vapor phase properties. The Poynting correction was used to calculate the reference state fugacity coefficient. Fig. 3 shows the formation of the minimum azeotrope (0.912 molar fraction of MEG) and close compositions of MEG in the vapor and liquid phases above the azeotrope point. Therefore, purification of this mixture above the azeotrope point using the conventional distillation technique is difficult.

The solid-liquid phase equilibrium was determined for the intended binary and ternary systems to assess the effect of adding a solvent in terms of the thermodynamics of crystallization and the nonideal behavior of the system. For this purpose, UNIFAC-DMD and NIST modified-UNIFAC predictive models were used to predict equilibrium temperatures and the NRTL model was employed to correlate the experimental data. The melting temperature of the MEG required for Equation (6) was assumed to be equal to its crystallization temperature. The measured crystallization temperature of MEG is 260.15 K. An enthalpy of fusion of 11630 J/mol was used for pure MEG according to the literature data (Parks & Kelley, 1925). The change in the composition of the mother liquor during progressing crystallization was estimated from the mass and material balance assuming the formation of pure crystals. The solute mass fraction and mass of mother liquor on a solvent-free basis

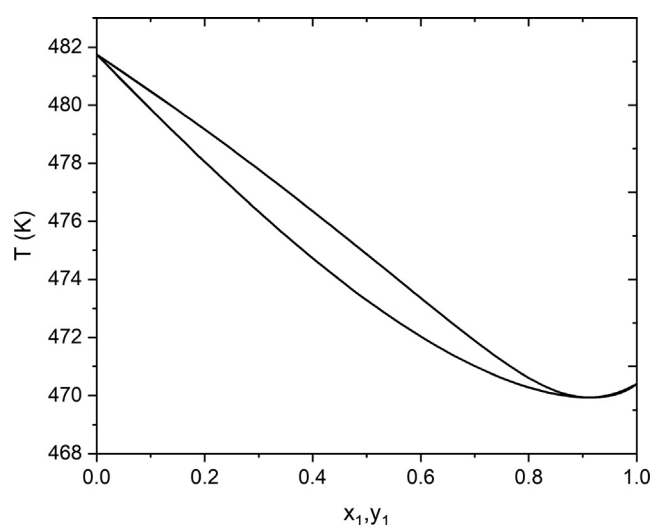


Fig. 3. Vapor-liquid equilibria of binary system MEG (1) + PD (2) at atmospheric pressure predicted using modified UNIFAC Dortmund model via Aspen Plus software.

are calculated using Equations (8) and (9) at different crystal yield values.

$$m'_f w'_{MEG,f} = m'_m w'_{MEG,m} + m_{cry} \quad (8)$$

$$m'_f = m'_m + m_{cry} \quad (9)$$

As the pure crystalline layer forms, the mass of the solvent in the melt should remain unchanged. Therefore, the change in solvent composition in the targeted ternary system ( $w_{s,m}$ ) in the remaining mother liquor ( $m_m$ ) was determined by:

$$w_{s,m} = \frac{m_f w_{s,f}}{m_m} \quad (10)$$

$$m_f = \frac{m'_f}{(1 - w_{s,f})} \quad (11)$$

$$m_m = m_f w_{s,f} + m'_m \quad (12)$$

Table 2 shows the theoretical and experimental equilibrium data in the specified compositions. All experimental measurements were repeated twice with a maximum deviation of  $\pm 0.1$  K from the average value. This data was used to optimized binary interaction parameters of the NRTL model (Table 1). Correlated data obtained using these parameters showed good agreement with experimental data. It should be noted that these parameters can only be employed for the binary and ternary systems examined. A larger amount of SLE data is required for a wider range of impurity and solvent compositions. The estimated SLE from the UNIFAC-DMD and NIST-modified UNIFAC models shows a higher deviation from the experimental data as the concentration of the solvent increases. The absolute average relative deviation (AARD) of the models is shown in Table 3.

#### 4.2. The effect of solvent composition on the thermodynamic driving force for crystallization

Thermodynamic models can be used to assess the effect of solvent composition on the thermodynamic driving force for crystallization. Fig. 4 shows that the required driving force to reach a particular equilibrium composition of MEG in the mother liquor is significantly lower in the binary system. Therefore, a lower undercooling degree must be applied to the system in order to reach the same crystallization yield in contrast to solvent-aided systems. This leads to a higher crystal growth rate for the binary mixture under similar operating conditions. Nonetheless, increasing the amount of solvent is not linked with an increase in the required driving force for crystallization, as increasing the solvent composition from 15 to 25 mol.% reduced this value in the solvent-aided systems. This can considerably offset the undesired reduction in the feed crystallization temperature due to the addition of a higher amount of solvent. The required operating temperature range for the examined systems to obtain desired equilibrium yield is shown in Fig. 5.

**Table 1**  
Calculated interaction parameters of the NRTL model for the ternary system of MEG (1) + PD (2) + acetone (3).

i-j	$a_{ij}$	$b_{ij}$	$\alpha$
1-2	-0.5	-250	0.2
2-1	1	950	
1-3	0.1	230	0.4
3-1	0.4	380	
2-3	0	-20	0.47
3-2	0	950	

**Table 2**  
SLE data for binary MEG (1) + PD (2) and ternary MEG (1) + PD (2) + acetone (3) systems.

$x_1$	$x_3$	$T_{EXP}$ [K]	$T_{UNIFAC-DMD}$ [K]	$T_{NIST-modified UNIFAC}$ [K]	$T_{NRTL}$ [K]
0.9904 <sup>a</sup>	0	259.35	259.69	259.69	259.68
0.9788	0	259	259.15	259.13	259.11
0.9696	0	258.63	258.73	258.68	258.65
0.8418 <sup>b</sup>	0.1500	253.86	253.57	253.54	254.03
0.7046	0.2802	250.68	249.44	249.35	250.56
0.6217	0.3588	248.83	247.63	247.44	249.01
0.7923 <sup>b</sup>	0.2000	252.45	251.96	251.94	252.67
0.6313	0.3550	249.26	247.97	247.87	249.33
0.5407	0.4423	248.05	246.61	246.39	248.03
0.7427 <sup>b</sup>	0.2500	251.35	250.56	250.55	251.52
0.5641	0.4237	248.70	247.07	246.94	248.48
0.4714	0.5138	247.45	246.26	245.92	247.45

<sup>a</sup> Feed composition for binary system of MEG (1) + PD(2).

<sup>b</sup> Feed composition of ternary system of MEG (1) + PD (2) + acetone (3) with different solvent compositions.

In this work, the maximum yield is defined as the highest achievable amount of crystallin material when the mother liquor reaches equilibrium. Crystallization yields in different compositions of mother liquor were determined based on equations 8–12. Subsequently, the equilibrium temperatures were calculated using the NRTL model.

#### 4.3. Influence of operating condition and solvent composition on crystal growth rate

Layer crystallization was performed at slow cooling rates of 0.67 and 1 K/h to avoid high supersaturation, which may result in the inclusion of impurities. The overall growth rate was measured based on the mass of the crystal layer,  $m_{cry}$ , growing vertically above the seed layer with a radius  $r$  over the crystallization time,  $\Delta t$ . The seed layer mass and solvent inclusions were excluded from the overall mass of the melted crystal. The density of the crystal,  $\rho_{cry}$ , is assumed to be equal to the density of pure MEG at 260.15 K ( $\rho_{MEG} = 1.27$  g/cm<sup>3</sup> (DIPPR 801, 2011)). All the experiments were repeated at least twice.

$$G = \frac{m_{cry}}{\pi r^2 \rho_{cry} \Delta t} \quad (13)$$

The crystal growth rate obtained with different compositions of solvent is shown in Fig. 6. As indicated in section 4.2, it is evident that the highest crystal growth rate was achieved in the binary system due to the higher thermodynamic driving force applied to the system under the same operating conditions. However, the observed subside in the growth rate of the crystal at the final temperature may be related to the increase in the thickness of the solid layer, which can act as an insulating layer between the cooled surface and the melt, thereby reducing the applied temperature.

On the other hand, the system with a solvent amount of 15 mol.% shows the lowest crystal growth rate at the beginning of crystallization where it was least expected, as the degree of supersaturation was almost equal in these three systems according to the estimated driving force. At the same degree of fundamental supersaturation, this difference can be attributed to the effect of transport phenomena and interfacial kinetics on the growth rate. The crystal growth rate can be limited by mass transfer by diffusion or processes at the interface. If diffusion is fast enough, the growth rate can be limited by surface integration (Beckmann, 2013). Viscosity is an important factor influencing diffusion in the bulk phase. The viscosity of the mother liquor at equilibrium states is shown in Fig. 7. In the solvent-aided systems, the highest viscosity can be observed for the system with 15 mol.% of solvent which can lead to slower mass transfer, thus leading to a slower growth rate.

However, as the viscosity decreased during progressing crystallization, the difference between growth rates also decreased. This implies that, due to the reduced viscosity in the solvent-aided systems examined, mass transfer by diffusion is no longer the limiting factor for crystal growth rate. This may further explain the minor effect of increasing the solvent composition from 20 to 25 mol.%

**Table 3**

Absolute average relative deviation between model results and experimental data.

	UNIFAC-DMD	NIST-modified UNIFAC	NRTL
AARD <sup>a</sup>	0.0034	0.0037	0.0005

$$^a \text{AARD} = \frac{1}{n} \sum_{i=1}^n \left| \frac{T_{\text{model}} - T_{\text{experiment}}}{T_{\text{experiment}}} \right|$$

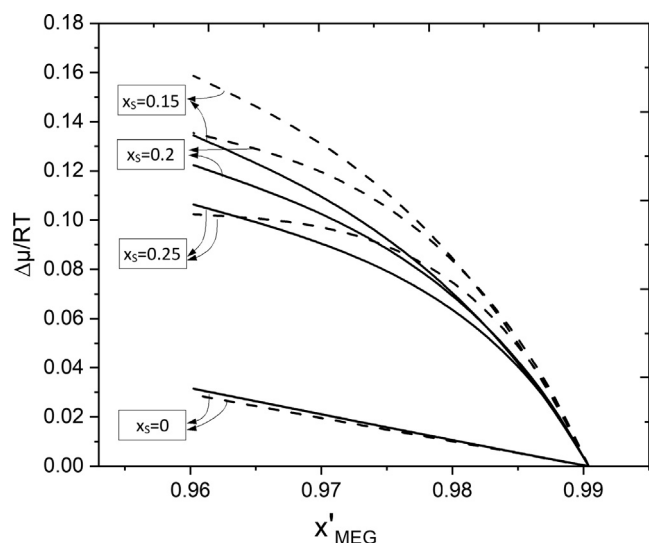


**Fig. 4.** Required driving force for crystallization against final equilibrium composition of the mother liquor on solvent-free basis. Dashed lines are the predicted values obtained from the UNIFAC-DMD model for systems with solvent composition of  $x_s$  in the feed. Solid lines are values determined by NRTL model for systems with solvent composition of  $x_s$  in the feed.

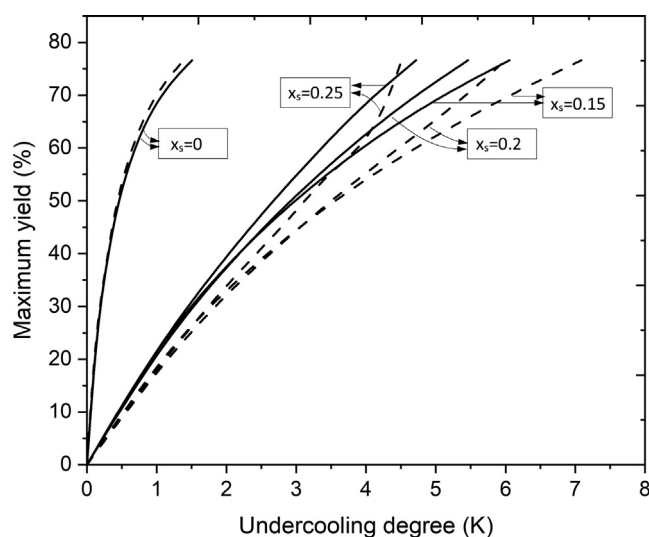


**Fig. 5.** Equilibrium yield against operating temperature range. Dashed lines are the predicted values obtained from the UNIFAC-DMD model for systems with solvent composition of  $x_s$  in the feed. Solid lines are values determined by the NRTL model for systems with a solvent composition of  $x_s$  in the feed.

on the crystal growth rate. The fast mass transfer in the liquid phase may minimize the kinetic incorporation of impurities into the crystal layer.

Further, the crystal growth can be controlled by the cooling rate, which can consequently influence the product purity. A higher growth rate due to an increase in cooling rate can result in a higher impurity inclusion in the crystal layer.

#### 4.4. Purification efficiency and crystallization yield:

Fig. 8 (a) shows that purities of 99.75 wt.%, 99.5 wt.%, and 99.3 wt.% were achieved at the examined final temperature and

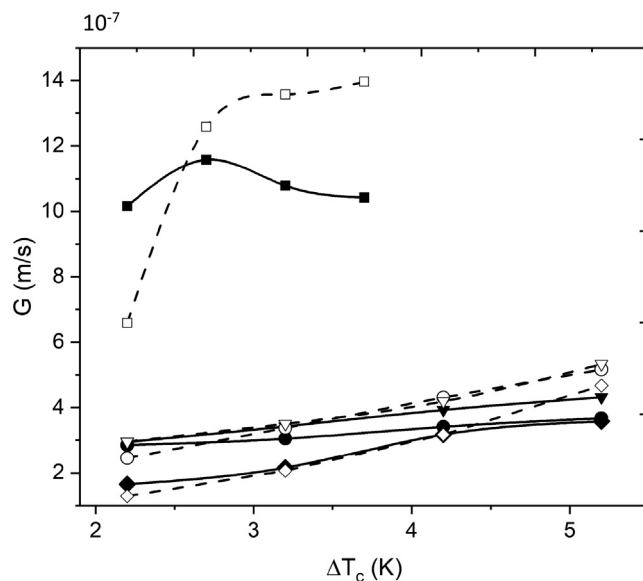


**Fig. 6.** Crystal growth rate in binary and ternary systems as a function of coolant undercooling degree. Straight solid lines and dotted lines are the measured layer growth rate at cooling rates of 0.67 and 1 K/h, respectively. The data marked with squares, diamonds, circles, and triangles represent systems with initial solvent molar composition of 0, 15, 20, and 25 mol.%, respectively.

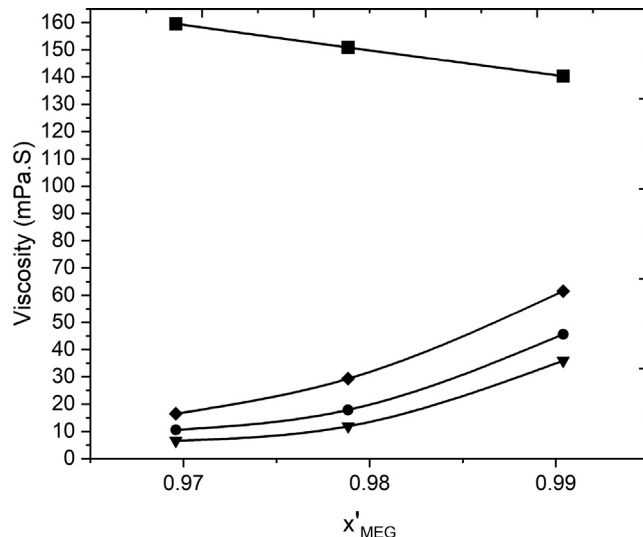


**Fig. 7.** Viscosity of bulk melt at equilibrium condition versus Solvent-free basis molar fraction of MEG for binary and ternary systems. The data marked with squares, diamonds, circles, and triangles represent systems with initial solvent molar composition of 0, 15, 20, and 25 mol.%, respectively.

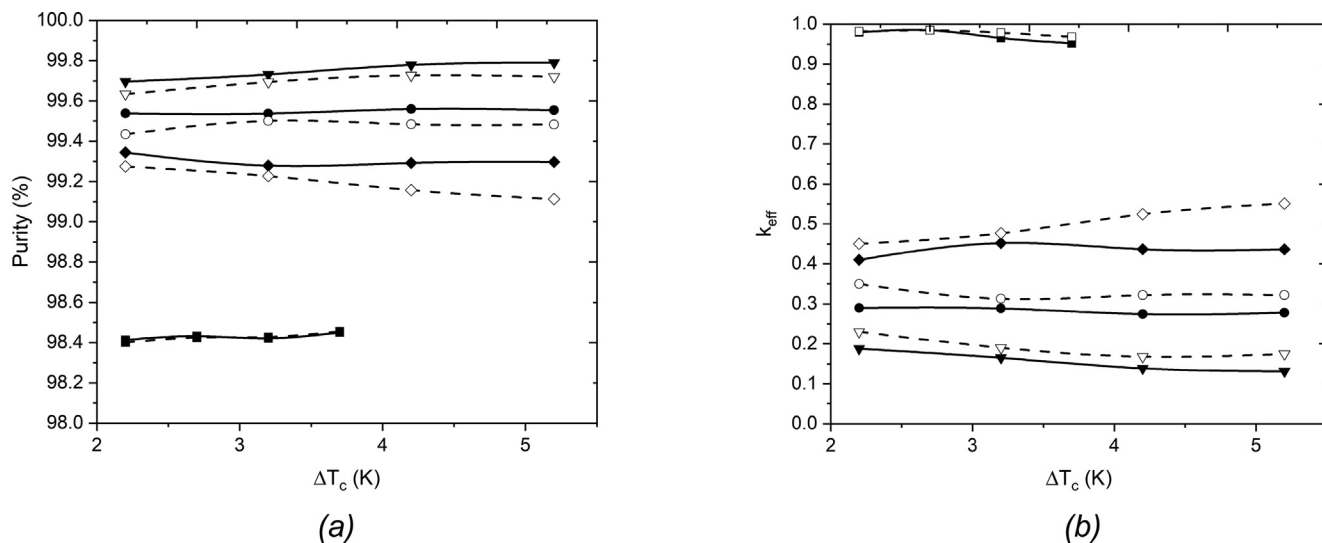


**Fig. 8.** Crystal purity (a) and distribution coefficient of impurity (b) in binary and ternary mixtures. Straight solid lines and dotted lines are measured layer growth rate at cooling rates of 0.67 and 1 K/h, respectively. The data marked with squares, diamonds, circles, and triangles represent systems with initial solvent molar composition of 0, 15, 20, and 25 mol.%, respectively.

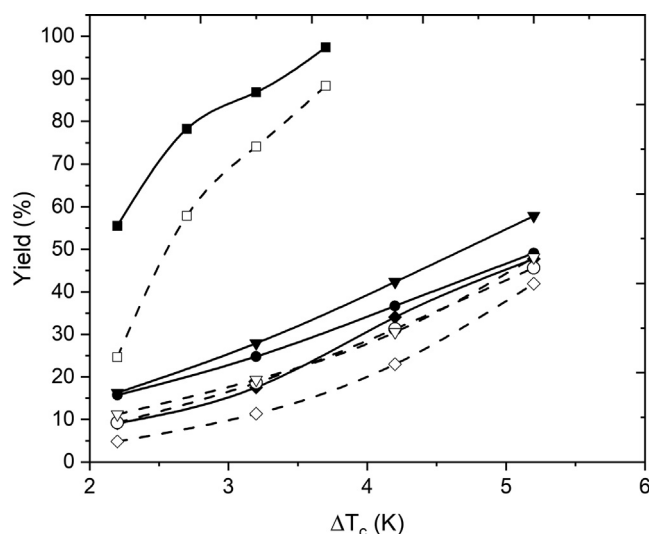


**Fig. 9.** Crystallization yield in binary and ternary mixtures. Straight solid lines and dotted lines are the measured layer growth rate at cooling rates of 0.67 and 1 K/h, respectively. The data marked with squares, diamonds, circles, and triangles represent systems with initial solvent molar composition of 0, 15, 20, and 25 mol.%, respectively.

cooling rate of 0.67 K/h in the system with a solvent composition of 25, 20, and 15 mol.%, respectively. The purity levels in this work are reported on a solvent-free basis. The results show that increasing the cooling rate to 1 K/h decreased the purity level of the final product by up to 0.2 wt.%. The maximum reduction in purity was observed in the system with the lowest amount of solvent, whereas increasing the amount of solvent reduced the effect of the cooling rate on the purity level.

The effective distribution coefficient is a parameter for evaluating purification efficiency, defined as the ratio of impurity content in the crystal to the impurity content in the feed. This parameter expresses the kinetic incorporation of impurities, comprising the effect of crystal growth rate and mass transfer limitations on the purity of crystals. A  $k_{eff}$  value close to one implies poor purification while lower values indicate higher separation efficiency.

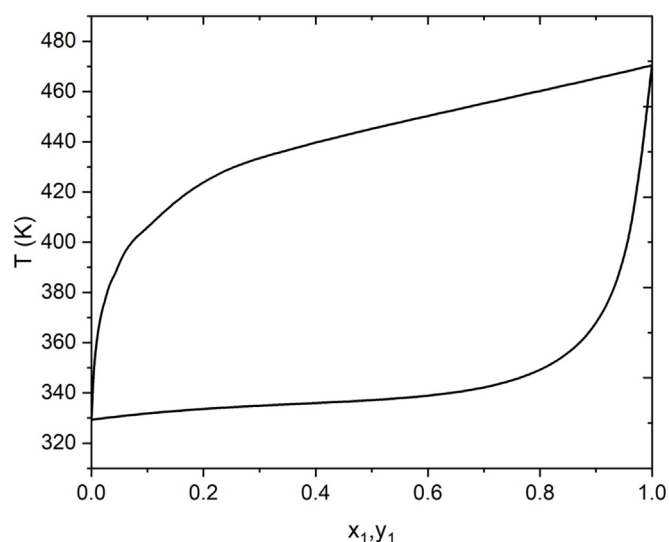


**Fig. 10.** VLE diagram of MEG (1) and acetone (2) estimated by the UNIFAC-DMD model at 101.325 kPa (Aspen Plus V11.0).

$$k_{eff} = \frac{w'_{imp,cr}}{w_{imp,f}} \quad (14)$$

Pure crystals with an effective distribution coefficient of near zero can be achieved at a low crystal growth rate and high mass transfer. High diffusivity may entail better transport of impurities from the crystal interface to the bulk phase (Beckmann, 2013). Fig. 8 (b) shows that, although a lower crystal growth rate favors the formation of pure crystals, higher purity was achieved in the systems with a higher concentration of the solvent in which the crystal growth rate was higher. This indicates that the kinetic incorporation of impurities into the crystal was not only controlled by the growth rate but also by the mass transfer in the bulk phase. Addition of solvent not only altered the applied driving force but also the mass transfer in the melt by increasing the diffusivity associated with reduced viscosity. Further, it can be seen that the purity of the crystal layer was not reduced at higher yields during progressing crystallization, as better transition of impurity hinders

liquid inclusions. This may further explain the lessened influence of the cooling rates examined on the purity level of the product in the system with a higher amount of solvent.

Fig. 9 shows the crystallization yield based on the weight ratio of MEG in the final product and feed. The lower kinetic yield in the ternary systems in contrast to the maximum yield estimated by the NRTL model indicates that the melt temperature ( $T_m$ ) is not in equilibrium with the coolant temperature ( $T_c$ ) under the applied cooling rates. Thus, an extension of crystallization time is required to achieve the equilibrium yield.

In the solvent-aided systems, a relation between the higher solvent content and higher purity level of the crystalline layer was observed regardless of the increase in crystal growth rate and the increase in yield during progressing crystallization. Although the effect of solvent interaction with the components in the bulk melt and surface of the crystal is a subject for further research, this relation may imply the important role of mass transfer in crystal purity along with crystal growth rate. Nevertheless, using a solvent in a system entails its recovery. The content of the crystal layer showed that the solvent remained mainly in the bulk melt. A maximum solvent occlusion of 6 wt.% occurred at the highest crystal growth rate. Fig. 10 shows the estimated vapor-liquid equilibrium data for the binary mixture of ethylene glycol and the solvent at atmospheric pressure using the models described in section 4.1. The results show no azeotrope formation. Thus, it is expected that the remaining solvent can be easily removed from the melted product by evaporation.

## 5. Conclusion

Solvent-aided layer melt crystallization enhanced purification in the studied binary system without the use of post-crystallization treatment techniques. The capability of modified group contribution models to predict the thermodynamics of crystallization was evaluated. A semi-empirical NRTL model was developed from solid-liquid equilibrium data concerning the liquid composition change during progressing crystallization that was in good agreement with the SLE experimental data. The model was used to determine the impact of solvent composition on the actual driving force for crystallization. The addition of solvent modified the crystallization thermodynamics, thereby changing the required range of operating temperatures. The impact of the thermodynamics and kinetics of crystallization on the purity of the final product was evaluated under different operating conditions. Although the addition of solvent reduced the viscosity, the actual driving force required for crystallization to obtain the same equilibrium yield in the solvent-aided system was higher, leading to a lower crystal growth rate at the same degree of undercooling and higher crystal purity. The crystal growth rates between  $6.5 \times 10^{-7}$  and  $14 \times 10^{-7}$  m/s for the binary system and between  $1.2 \times 10^{-7}$  and  $5.3 \times 10^{-7}$  m/s for the solvent-aided systems were obtained under the operating conditions examined. Enhanced mass transfer associated with the reduced viscosity near the liquidus line and lower crystal growth rate were favorable for increasing the purity of the crystalline layer.

### CRedit authorship contribution statement

**M. Ila:** Conceptualization, Investigation, Visualization, Writing – original draft, Methodology, Validation, Writing – review & editing.  
**M. Louhi-Kultanen:** Conceptualization, Writing – review & editing, Supervision, Funding acquisition.

## Data availability

Data will be made available on request.

## Declaration of Competing Interest

The authors declare that they have no known competing financial interests or personal relationships that could have appeared to influence the work reported in this paper.

## Acknowledgements

This work made use of the Bioeconomy and RawMatters facilities at Aalto University, Espoo/Finland. This project has received funding from the European Union's Horizon 2020 research and innovation programme under grant agreement No 869993.

## References

- Beckmann, W., 2013. *Crystallization: Basic Concepts and Industrial Applications*. Wiley-VCH Verlag GmbH & Co. KGaA, Weinheim.
- Cong, S., Liu, Y., Li, H., Li, X., Zhang, L., Wang, L., 2015. Purification and separation of durenene by static melt crystallization. *Chin. J. Chem. Eng.* 23 (3), 505–509. <https://doi.org/10.1016/j.cjche.2014.11.018>.
- DIPPR 801, 2011. Design Institute for Physical Property Research/AIChE.
- Eisenbart, F.J., Ulrich, J., 2015. Solvent-aided layer crystallization—Case study glycerol–water. *Chem. Eng. Sci.* 133, 24–29. <https://doi.org/10.1016/j.ces.2014.12.060>.
- Feng, H., Wang, N., Huang, X., Wang, T., Zhou, L., Hao, H., 2023. Recent progress in melt crystallization. *Chem. Eng. Res. Des.* 190, 268–281. <https://doi.org/10.1016/j.cherd.2022.12.030>.
- Gmehling, J., Li, J., Schiller, M., 1993. A modified UNIFAC model. 2. Present parameter matrix and results for different thermodynamic properties. *Ind. Eng. Chem. Res.* 32 (1), 178–193. <https://doi.org/10.1021/ie00013a024>.
- Haynes, W.M., Lide, D.R., Bruno, T.J., 2017. *CRC Handbook of Chemistry and Physics, Ninety-seven ed.* CRC Press, Boca Raton.
- Kang, J.W., Diky, V., Frenkel, M., 2015. New modified UNIFAC parameters using critically evaluated phase equilibrium data. *Fluid Phase Equilib.* 388, 128–141. <https://doi.org/10.1016/j.fluid.2014.12.042>.
- Kang, J.W., Diky, V., Frenkel, M., 2017. Corrigendum to “New modified UNIFAC parameters using critically evaluated phase equilibrium data” [*Fluid Phase Equilib.* 388 (2015) 128–141]. *Fluid Phase Equilib.* 440, 122–123. <https://doi.org/10.1016/j.fluid.2017.02.014>.
- Li, X., Wang, R., Na, J., Li, H., Gao, X., 2018. Reversible Reaction-Assisted Intensification Process for Separating the Azeotropic Mixture of Ethanediol and 1,2-Butanediol: Reactants Screening. *Ind. Eng. Chem. Res.* 57 (2), 710–717. <https://doi.org/10.1021/acs.iecr.7b04012>.
- Micovic, J., Beierling, T., Lutze, P., Sadowski, G., Górak, A., 2013. Design of hybrid distillation/melt crystallisation processes for separation of close boiling mixtures. *Chem. Eng. Process.* 67, 16–24. <https://doi.org/10.1016/j.ccep.2012.07.012>.
- Mullin, J.W., 2001. *Crystallization, fourth ed.* Butterworth-Heinemann, Oxford.
- Parks, G.S., Kelley, K.K., 1925. Thermal data on organic compounds. II. The heat capacities of five organic compounds. The entropies and free energies of some homologous series of aliphatic compounds. *J. Am. Chem. Soc.*, 47(8), 2089–2097. [10.1021/ja01685a003](https://doi.org/10.1021/ja01685a003).
- Renon, H., Prausnitz, J.M., 1968. Local compositions in thermodynamic excess functions for liquid mixtures. *AIChE J.* 14 (1), 135–144. <https://doi.org/10.1002/aic.690140124>.
- Valavi, M., Svård, M., Rasmuson, Å.C., 2016. Improving Estimates of the Crystallization Driving Force: Investigation into the Dependence on Temperature and Composition of Activity Coefficients in Solution. *Cryst. Growth Des.* 16 (12), 6951–6960. <https://doi.org/10.1021/acs.cgd.6b01137>.
- Walas, S.M., 1985. *Phase equilibria in chemical engineering*. Butterworth Publishers, Stoneham.
- Wang, T., Li, X., Dong, J., 2020. Ethylene Glycol Purification by Melt Crystallization: Removal of Short-Chain Glycol Impurities. *Ind. Eng. Chem. Res.* 59 (18), 8805–8812. <https://doi.org/10.1021/acs.iecr.0c00347>.
- Yu, H., Ye, Q., Xu, H., Dai, X., Suo, X., Li, R., 2016. Investigation on Thermodynamics in Separation for Ethylene Glycol + Neopentyl Glycol System by Azeotropic Distillation. *J. Chem. Eng. Data* 61 (7), 2330–2334. <https://doi.org/10.1021/acs.jced.5b01044>.
- Yue, H., Zhao, Y., Ma, X., Gong, J., 2012. Ethylene glycol: Properties, synthesis, and applications. *Chem. Soc. Rev.* 41 (11), 4218–4244. <https://doi.org/10.1039/c2cs15359a>.
- Zhang, L., Wu, W., Sun, Y., Li, L., Jiang, B., Li, X., Yang, N., Ding, H., 2013. Isobaric Vapor-Liquid Equilibria for the Binary Mixtures Composed of Ethylene Glycol, 1,2-Propylene Glycol, 1,2-Butanediol, and 1,3-Butanediol at 10.00 kPa. *J. Chem. Eng. Data* 58 (5), 1308–1315. <https://doi.org/10.1021/jc400082c>.